Traveling-Wave IMPATT Amplifiers and Oscillators

RICHARD K. MAINS, MEMBER, IEEE, AND GEORGE I. HADDAD, FELLOW, IEEE

Abstract—**Traveling-wave IMPATT oscillators and amplifiers are analyzed using a large-signal transmission-line model. A specific case for a GaAs structure at 33.7 GHz is examined in detail. General equations relating to the design and expected power output from these devices are also developed. It is concluded that more RF power can be generated by traveling-wave structures than is obtainable from discrete IMPATT devices.**

I. Introduction

In 1968, MIDFORD and Bowers [1] presented experimental results for an elongated Si IMPATT ($L = 4$–10 mm) operated as a traveling-wave amplifier in the form of a strip transmission line. An analysis of this type of structure was provided by Hambleton and Robson [2] in 1973. In their analysis, Maxwell's equations were solved in conjunction with a simplified, uniform IMPATT device model. Fig. 1 shows the geometry considered in the analysis. Region 1 in this figure is the active device region and region 2 is the substrate region. The results of this analysis showed that this problem can be treated approximately as an equivalent transmission-line problem, where the series resistance R_s and series inductance L_s are given by

$$R_s = \omega\mu_0 \frac{b + a + d + \delta_m}{w} \cdot \frac{\dfrac{\delta_m}{b} + \dfrac{2}{3}\left(\dfrac{d}{b}\right)\left(\dfrac{d}{\delta_s}\right)^2 + \dfrac{2}{3}\left(\dfrac{a}{b}\right)\left(\dfrac{a}{\delta_p}\right)^2}{\left(1 + \dfrac{d+a}{b} + \dfrac{\delta_m}{b}\right)} \ (\Omega/\text{m}) \quad (1)$$

and

$$L_s = \mu_0 \frac{b + a + d + \delta_m}{w} \ (\text{H/m}). \quad (2)$$

In the preceding equations, a is the thickness in the x-direction of the p^+ layer in Fig. 1 and δ_m, δ_s, and δ_p are the skin depths in the metal contacts, the n^+ layer, and the p^+ layer, respectively, given by

$$\delta_i = \left(\frac{2}{\omega\mu_0\sigma_i}\right)^{1/2} \ (\text{m}) \quad (3)$$

Manuscript received January 2, 1986; revised April 26, 1986. This work was supported in part by the Naval Weapons Center.

The authors are with the Solid-State Electronics Laboratory, Department of Electrical Engineering and Computer Science, The University of Michigan, Ann Arbor, MI 48109.

IEEE Log Number 8609606.

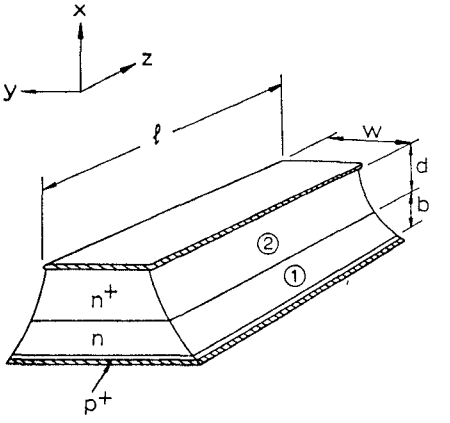

Fig. 1. Distributed IMPATT structure. Region 1 is the active device, region 2 is the substrate, and the shaded areas are the metal contacts (from Hambleton and Robson [2]).

where σ_i ($\Omega^{-1}\text{m}^{-1}$) is the conductivity of the appropriate region i.

The equivalent transmission line is loaded by a shunt admittance Y_s where

$$Y_s = w[G_D + jB_D] \ (\Omega^{-1}/\text{m}). \quad (4)$$

In (4), $Y_D = G_D + jB_D$ ($\Omega^{-1}\text{m}^{-2}$) is the IMPATT diode admittance per unit area.

Analyses were carried out in [2], using these equations, that showed, in particular, the effects of the thicknesses and resistivities of the n^+ and p^+ regions in Fig. 1 on expected device performance.

In 1978, Franz and Beyer [3] analyzed this structure by solving Maxwell's equations in conjunction with a distributed small-signal model for the IMPATT diode. Again, in this and in their subsequent paper [4], they concluded that the problem may be regarded, to a good approximation, as that of an effective transmission line. Also, they indicated [4] that an effective large-signal analysis might be carried out by allowing the shunt admittance Y_s to be a function of the RF voltage along the transmission line, rather than a constant. Their analysis was limited by the fact that they assumed the substrate to be a perfect conductor, so that the analysis does not contain the effects of substrate thickness and resistivity included in Hambleton and Robson's earlier work [2].

In 1983, Bayraktaroglu and Shih [5] reported experimental results for distributed GaAs IMPATT oscillators. Output powers obtained were 1.5 W at 22 GHz, 0.5 W at 50

0018-9480/86/0900-0965$01.00 ©1986 IEEE

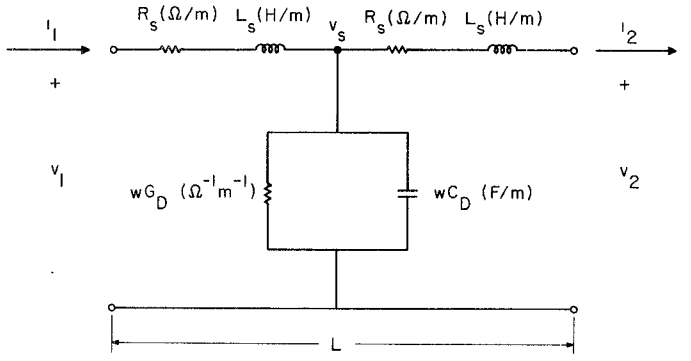

Fig. 2. Section of length L used to model the distributed IMPATT.

GHz, and approximately 7 mW at 89 GHz. Based on the results of the present investigation, it is not believed that the structure presented in [5] was optimum for traveling-wave IMPATT operation, so that higher output powers are expected in the future.

In 1985, Fukuoka and Itoh [6] carried out a field analysis of traveling-wave IMPATT structures. A small-signal IMPATT device model was used where diffusion was neglected and drift at saturated velocities was assumed. The effects of losses in the substrate and conductor regions were included in their analysis.

A field analysis incorporating a more realistic device model has not yet been carried out. In this paper, a more elaborate device model is incorporated in a simplified, TEM transmission-line formulation of the problem.

II. Description of the Model and Method of Analysis

The distributed IMPATT structure is divided into a series of uniform sections of length L. L is made small enough so that the RF voltage does not vary appreciably within each section. In these calculations, L was chosen to be about $\lambda/100$, where λ is the wavelength of the traveling waves along the line. Fig. 2 shows the representation used for each section. In this figure, R_s and L_s are obtained from (1) and (2). $G_D(v_s)$ is the diode conductance in (Ω^{-1}/m^2) obtained from large-signal simulation results. G_D depends on v_s, the RF voltage magnitude at the center of the section. Similarly, the diode susceptance $B_D(v_s) = \omega C_D(v_s)$ is characterized by the capacitance $C_D(v_s)$ in F/m^2, also a function of v_s. Therefore, $w(G_D + j\omega C_D)$ gives the diode conductance per unit length, since w is the width of the structure (see Fig. 1). The $ABCD$ parameters for the section of Fig. 2 are

$$\begin{aligned} A &= 1 + Y_s(R_s + j\omega L_s)\frac{L^2}{2} \\ B &= (R_s + j\omega L_s)L + Y_s(R_s + j\omega L_s)^2\frac{L^3}{4} \\ C &= Y_s L \\ D &= A \end{aligned} \tag{5}$$

where ω is the angular frequency of the voltage and current waves at any point along the line and Y_s is given by (4). It is assumed that Y_s is constant within each section since L is small. The distributed IMPATT device is modeled as a cascade of sections of this type, where Y_s varies from section to section according to v_s.

Although the $ABCD$ parameters in (5) are functions of the RF voltage, useful information is also obtained by considering the uniform transmission-line case for constant Y_s (chosen, for example, at the RF voltage where maximum diode efficiency is obtained). The characteristic impedance and propagation factor for the uniform line are given by

$$Z_0 = \left(\frac{R_s + j\omega L_s}{w(G_D + jB_D)}\right)^{1/2} (\Omega) \tag{6}$$

and

$$\begin{aligned} \gamma &= \alpha + j\beta \\ &= [(R_s + j\omega L_s)(G_D + jB_D)w]^{1/2}(m^{-1}). \end{aligned} \tag{7}$$

In (7), α is the attenuation (or gain) factor and $\beta = 2\pi/\lambda$ is the phase factor for the line. Since ωL_s and wB_D are typically an order of magnitude larger then R_s and wG_D

$$\mathrm{Im}(\gamma) = \beta = 2\pi/\lambda \cong \sqrt{\omega L_s B_D w}\ (m^{-1}). \tag{8}$$

B_D is approximately ωC_D which, for punched-through devices, does not vary appreciably with V_{RF}. Then (8) is a good approximation for the large-signal case, where V_{RF} varies along the transmission line. In contrast, the gain factor α varies significantly with device negative conductance G_D.

Equation (8) is used as follows. First, it is assumed that the IMPATT diode has been characterized at the desired frequency of operation so that B_D and ω are known. Then (8) can be evaluated from the geometry of the structure and the conductivities of the n^+, p^+, and metal layers. This gives λ, which must be known to determine the correct length of an oscillator for operation at the desired frequency.

Equation (6) may be used to estimate the maximum obtainable power from a traveling-wave IMPATT structure, either for the oscillator or the amplifier case. If V_{max} denotes the (peak) value of V_{RF} for which maximum device efficiency is obtained and $G_D(V_{max}) + jB_D(V_{max})$ denotes the device shunt admittance per unit area at this RF voltage, maximum power is obtained when the voltage at the load is approximately V_{max} and when the line is terminated in its characteristic impedance so that no power is reflected at the load. Therefore, the maximum obtainable RF power is

$$(P_{RF})_{max} = \frac{V_{max}^2}{2}\frac{\mathrm{Re}(Z_0)}{\mathrm{Re}^2(Z_0) + \mathrm{Im}^2(Z_0)} \tag{9}$$

where Z_0 is evaluated using $G_D(V_{max})$, $B_D(V_{max})$.

Fig. 3 shows the configuration used for the large-signal analysis. The $ABCD$ network represents a cascade of all the individual sections of the type shown in Fig. 2 along the distributed structure. Power is extracted at the right-hand side, in the terminating impedance Z_T. For the

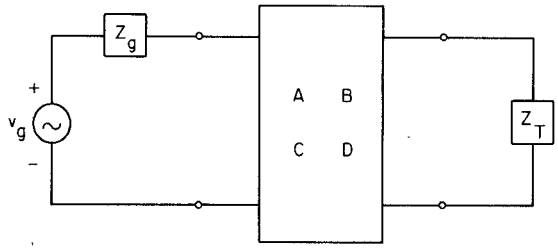

Fig. 3. Overall configuration for the distributed IMPATT amplifier analysis. Box labeled *ABCD* is a cascade of subsections of the type shown in Fig. 2. (For the oscillator case, $v_g = 0$ and Z_g is either an open or a short circuit.)

oscillator case, $v_g = 0$ and Z_g will nearly be either a short or open circuit. For the amplifier case, $v_g \neq 0$, $Z_g = 0$, and $Z_T \cong Z_0$ so that maximum power is transferred to the load. The first step is to read in $G_D(V_{RF})$ and $B_D(V_{RF})$, the diode large-signal admittance data. Then, an initial guess $V_{RF}^{(0)}$ is made as to the RF voltage distribution along the transmission line. With $V_{RF}^{(0)}$ known in each section, $Y_S(V_{RF}^{(0)})$ is determined by interpolating in V_{RF} between discrete values read in. Then the circuit of Fig. 3 can be solved for the *ABCD* parameters and the RF voltage variation along the line, yielding the next guess $V_{RF}^{(1)}$. This process is repeated until the values $V_{RF}^{(j)}$ are very close to the values $V_{RF}^{(j-1)}$ obtained for the previous iteration; at this point, the solution is converged and various quantities of interest, such as output power and overall efficiency, are computed.

At each iteration for the amplifier case, $|v_g|$ is set so that $|V_{RF}|$ at the load is equal to a specified maximum value read in as input $(V_{RF})_{max}$. Therefore, the final solution will have the RF voltage magnitude $(V_{RF})_{max}$ at the load. Z_T is set to the characteristic impedance of the transmission line calculated using $(V_{RF})_{max}$. For the oscillator case, $(V_{RF})_{max}$ at the load is also imposed; however, Z_T is set to the negative of the input impedance exhibited by the *ABCD* network terminated in Z_g (see Fig. 3). The impedance required to obtain oscillation at the desired frequency is

$$Z_T = -\frac{B + DZ_g}{A + CZ_g}. \tag{10}$$

Therefore, if Z_g is an open circuit, the oscillator is terminated in $-D/C$, whereas if Z_g is a short, the termination is $-B/A$. These are the two cases considered here.

After a converged solution is obtained for either the amplifier or oscillator case, the RF power delivered to the load is calculated as

$$(P_{RF})_L = \frac{1}{2}|V_T|^2 \frac{R_T}{R_T^2 + X_T^2} \tag{11}$$

where V_T is the (phasor) RF voltage at $Z_T = R_T + jX_T$. The overall efficiency is calculated as

$$\eta = \frac{(P_{RF})_L - (P_{RF})_{in}}{P_{dc}} \tag{12}$$

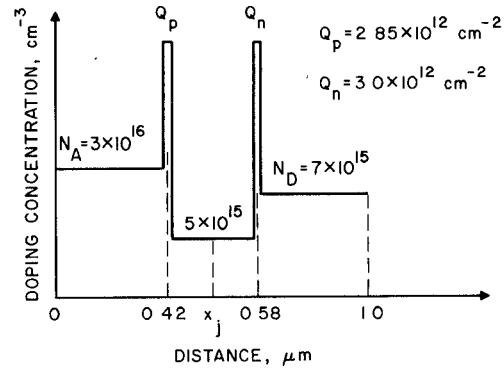

Fig. 4. IMPATT doping profile used for the distributed IMPATT oscillator simulations.

where P_{dc} is the dc power input to layers 1 and 2 and the p^+ layer in Fig. 1, and $(P_{RF})_{in}$ is the RF power input on the left-hand side (zero for the oscillator when $Z_g = 0$ or $Z_g = \infty$).

For all the simulations carried out, it was assumed that the shunt IMPATT device is biased with a constant dc current density J_{dc} A/cm^2 and that the device temperature is constant. Since the RF voltage varies along the line, the dc operating voltage must also vary under these conditions. However, if the entire line is dc connected as indicated in Fig. 1, the operating voltage is forced to be constant, which would produce variations in J_{dc} and T along the device length. For the punched-through device considered, the operating voltage variation versus V_{RF} is slight (24.43 V to 24.97 V) so that the constant current and temperature approximation may not introduce appreciable error. Also, the line could be dc isolated at regular intervals to allow for operating voltage variation. This would, however, introduce undesirable reflections of the traveling waves.

III. Results

Fig. 4 shows the GaAs double-Read IMPATT doping profile used for the shunt device, where the distance axis of Fig. 4 is along the x-direction of Fig. 1. To characterize this device, simulations at $f = 33.7$ GHz, $T = 500$°K, and $J_{dc} = 5.8$ kA/cm^2 were carried out versus V_{RF} using the energy-momentum transport model [7]. Table I presents the calculated device admittance $G_D + jB_D$ and operating voltage V_{op}. An optimum efficiency of $\eta = 25.46$ percent was obtained for the device at $V_{RF} = 15$ V. (Beyond 15 V, the efficiency drops; however, it is difficult to obtain solutions using the energy-momentum simulation in this region. In all the traveling-wave simulations carried out here, $|V_{RF}| \leq 15$ V.) For a discrete device operating at $V_{RF} = 15$ V, choosing a device area $A = 6.77 \times 10^{-5}$ cm^2 results in a negative resistance of 1 Ω and a power output of 2.44 W. The width of the distributed device, w in Fig. 1, was chosen as $w = \sqrt{A} = 8.23 \times 10^{-3}$ cm. The choice of width is arbitrary in this analysis, since transverse wave modes are not considered. Output power obtained scales linearly with w and impedance values are inversely proportional to the w value used.

TABLE I
LARGE-SIGNAL CHARACTERIZATION OF THE IMPATT DEVICE OF FIG. 4 AT $T = 500°$ K, $J_{dc} = 5.8$ kA/cm^2, AND $f = 33.7$ GHz

V_{RF} (V)	G_D (Ω^{-1}cm^{-2})	B_D (Ω^{-1}cm^{-2})	V_{op} (V)
4	- 667.3	1.884×10^3	24.07
8	- 538.0	2.003×10^3	24.55
10	- 481.5	2.059×10^3	24.90
12	- 420.0	2.097×10^3	24.97
12.5	- 399.3	2.112×10^3	24.97
13	- 385.2	2.122×10^3	24.96
14	- 347.6	2.146×10^3	24.83
15	- 320.7	2.153×10^3	24.43

The width and resistivity of the n^+ layer in Fig. 1 may be chosen as follows (the width of the p^+ layer is chosen to be zero in these simulations). The uniform line approximation is used and G_D, B_D for a particular V_{RF} are selected from Table I. A particular resistivity for the n^+ layer is tried, which determines δ_s in (1). Then the thickness d is varied and for each value of d, (7) is solved to determine α and $\lambda = 2\pi/\beta$. If α and β are of opposite sign, for this choice of n^+ resistivity and thickness, the line exhibits a gain per wavelength given by $e^{-(\alpha\lambda)}$. For some value of d, $e^{-(\alpha\lambda)}$ will be maximized. This value d_{opt} is the optimum n^+ layer thickness for that choice of n^+ resistivity and results in the most efficient traveling-wave structure. Examining $e^{-(\alpha\lambda)}$ for different resistivity values then determines the overall most efficient structure.

In addition to the optimum d_{opt} for each n^+ resistivity and G_D, B_D (i.e., V_{RF}) combination, the range of d for which the device will exhibit gain may be calculated from the following considerations. To exhibit gain, $\alpha + j\beta$ of (7) must lie in the second or fourth quadrants of the complex plane. This condition is equivalent to γ^2 being in the third or fourth quadrants or

$$\mathrm{Im}(\gamma^2) = w(\omega L_s G_D + R_s B_D) < 0. \tag{13}$$

Equation (13), nonlinear in d, is solved for the range of d over which the inequality is satisfied. Table II presents these results for two V_{RF} values and for substrate resistivities varying from 5×10^{-3} to 5×10^{-6} Ω-m.

The highest gain/wavelength values are obtained for high substrate resistivities, which is consistent with the results presented in [2]. It may be objected that for the $\rho = 5\times10^{-3}$ case, the n^+ concentration is actually below the n concentration for the IMPATT doping profile so that, for this case, the diode depletion-layer edge would extend much farther on the n side than is indicated in Fig. 4. To realize this case, a thin higher-doped layer would have to be inserted between the diode n-type drift region and the higher resistivity substrate. This layer would define the diode depletion-layer edge.

TABLE II
OPTIMUM SUBSTRATE THICKNESS, RANGE OF SUBSTRATE THICKNESS FOR WHICH GAIN IS OBTAINED, WAVELENGTH AND GAIN/WAVELENGTH FOR VARIOUS V_{RF}, ρ_s COMBINATIONS

V_{RF} (V)	ρ_s (Ω-m)	n^+ (cm^{-3})	d_{opt} (μm)	d_L-d_H (μm)	λ (cm)	$e^{-(\alpha\lambda)}$
15	5×10^{-3}	3.12×10^{15}	21	1.04-91.1	5.53×10^{-2}	1.48
15	5×10^{-4}	3.12×10^{16}	10	1.05-28.4	7.75×10^{-2}	1.37
15	5×10^{-5}	3.12×10^{17}	4	1.1-8.55	0.113	1.21
15	5×10^{-6}	3.12×10^{18}	1.65	1.33-2.0	0.150	1.01
4	5×10^{-6}	3.12×10^{18}	1.70	0.0-4.63	0.156	1.85
4	5×10^{-4}	3.12×10^{16}	10	0.0-44.9	8.17×10^{-2}	2.53

TABLE III
CHARACTERISTIC IMPEDANCE AND MAXIMUM OUTPUT POWER FOR DIFFERENT COMBINATIONS OF V_{RF}, ρ_s, AND d

V_{RF} (V)	ρ_s (Ω-m)	d (μm)	Z_o (Ω)	$(P_{RF})_{max}$ (W)
15	5×10^{-4}	10	4.508-j0.4408	24.72
15	5×10^{-5}	4	3.094-j0.3661	35.86
15	5×10^{-6}	2	2.448-j0.3644	44.96
4	5×10^{-4}	9	4.43-j0.8689	1.74

Table III shows the characteristic impedance Z_0 for the uniform line case for different combinations of V_{RF}, ρ_s, and d. Also shown are estimates of the maximum RF power available from each structure according to (9) ($(V_{RF})_{max} = V_{RF}$ in Table III). It is seen that the most power is obtained for the smallest substrate resistivity. However, several problems with this structure should be brought out. From Table II, the case with $\rho_s = 5\times10^{-6}$ Ω - m has the smallest gain/wavelength factor, which results in the smallest overall efficiency η for this structure; therefore, it is most likely to suffer from overheating. Also, this case has the smallest range of d over which gain is expected; practically, this means that very tight tolerances must be maintained in fabricating this structure, and any deviations from the design calculations (for example, in the device characterization G_D and B_D) may easily result in no gain at all. A further disadvantage of this structure is that $\mathrm{Re}(Z_0)$ is small so that it is more difficult to match at the load. For these reasons, it is better to design the structure for maximum efficiency (i.e., maximum $e^{-(\alpha\lambda)}$) rather than maximum power.

Fig. 5 shows the results obtained for RF power and overall efficiency for the oscillator case versus length in units of λ. Both the $Z_g = 0$ and $Z_g = \infty$ cases lie on these curves. Curves 1, 2, and 3 correspond to the combinations ($\rho_s = 5\times10^{-4}$ Ω - m, $d = 10$ μm), ($\rho_s = 5\times10^{-5}$ Ω - m, $d = 4$ μm), and ($\rho_s = 5\times10^{-6}$ Ω - m, $d = 2$ μm), respectively. As already estimated, the case with lowest substrate

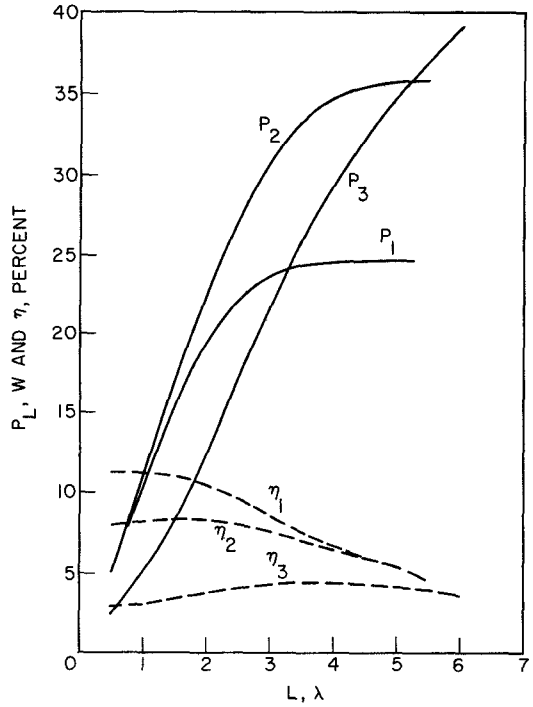

Fig. 5. Power output and efficiency versus oscillator length for both shorted and open oscillators. Curves labeled 1 are for ($\rho_s = 5\times10^{-4}$ $\Omega-$m, $d = 10$ μm), curves 2 are for ($\rho_s = 5\times10^{-5}$ $\Omega-$m, $d = 4$ μm), and curves 3 are for ($\rho_s = 5\times10^{-6}$ $\Omega-$m, $d = 2$ μm).

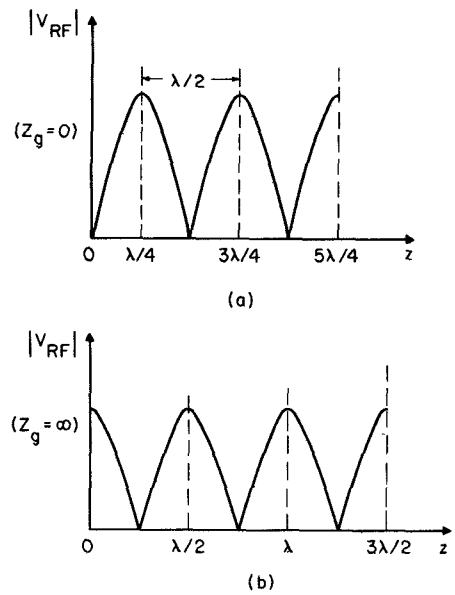

Fig. 6. Distribution of $|V_{RF}|$ along the transmission line for the oscillator case with (a) $Z_g = 0$ and (b) $Z_g = \infty$.

resistivity exhibits highest RF power but lowest efficiency, while the high substrate resistivity case gives lower power but highest overall efficiency. The RF power saturates at approximately $L = 3.5\lambda$ for the highest resistivity case and approximately 5λ for the $\rho_s = 5\times10^{-5}$ $\Omega-$m case (it should be recalled that λ is different for the three cases, according to Table II). The reason for the power saturation is explained in terms of the forward and reverse traveling waves along the transmission line. Fig. 6 shows the ideal

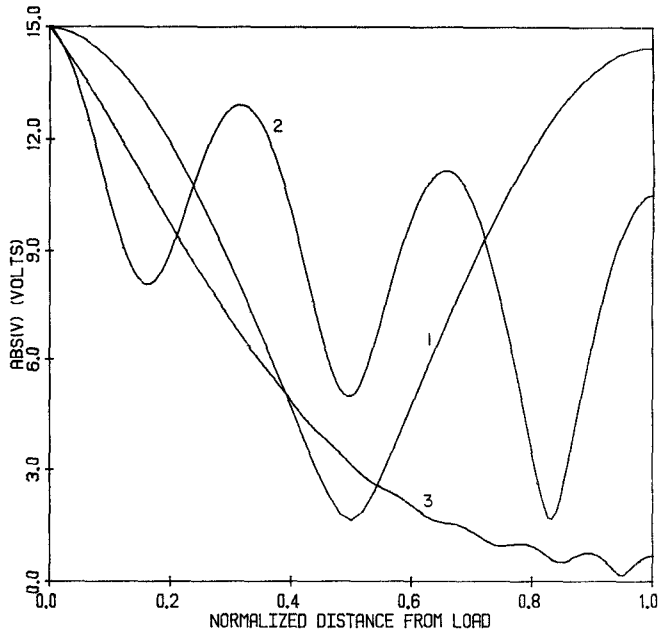

Fig. 7. $|V_{RF}|$ versus normalized distance from the load for the open-circuited oscillator case for (1) $L = \lambda/2$, (2) $L = (3\lambda/2)$, and (3) $L = 5\lambda$.

RF voltage distribution for the shorted and open oscillator cases. These curves presuppose complete reflection at the load, since otherwise the voltage nulls would not go exactly to zero. In the actual oscillator, not all the power will be reflected at the load and, in fact, as more power is extracted from the oscillator, the RF voltage waveforms will less resemble those of Fig. 6.

Fig. 7 shows actual RF voltage distributions for the $\rho_s = 5\times10^{-4}$ $\Omega-$m, $d = 10$ μm case for different values of oscillator length. The oscillator is open circuited at the normalized distance $= L/L = 1$ and $(V_{RF})_{max} = 15$ V at the load (0) for each case. It is seen that as the oscillator becomes longer, the waveforms more resemble those expected for the amplifier case. The terminating impedance decreases as L increases and approaches the characteristic impedance Z_0 so that not enough power is reflected to produce the ideal waveforms of Fig. 6.

In Fig. 5, case 3 for $\rho_s = 5\times10^{-6}$ $\Omega-$m is still not saturated at $L = 6\lambda$. In fact, it was difficult to obtain converged solutions for this case for larger L, reflecting the instability already discussed in relation to Table II.

The terminating impedance for the cases shown in Fig. 5 is nearly real and is approximately given by

$$R_T \cong \frac{(V_{RF})^2_{max}}{2P_L} = \frac{112.5}{P_L}\ \Omega. \tag{14}$$

(This equation assumes that the imaginary part X_T is brought to zero by slight adjustment of the oscillator length and/or operating frequency.) For example, the most efficient oscillator structure in Fig. 5 requires a terminating resistance $R_T = 21.7$ Ω for $L = \lambda/2$ and $R_T = 4.55$ Ω for $L = 5\lambda$.

Fig. 8 shows results for the amplifier case with $\rho_s = 5\times10^{-4}$ $\Omega-$m and $d = 10$ μm for different values of $(V_{RF})_{max}$

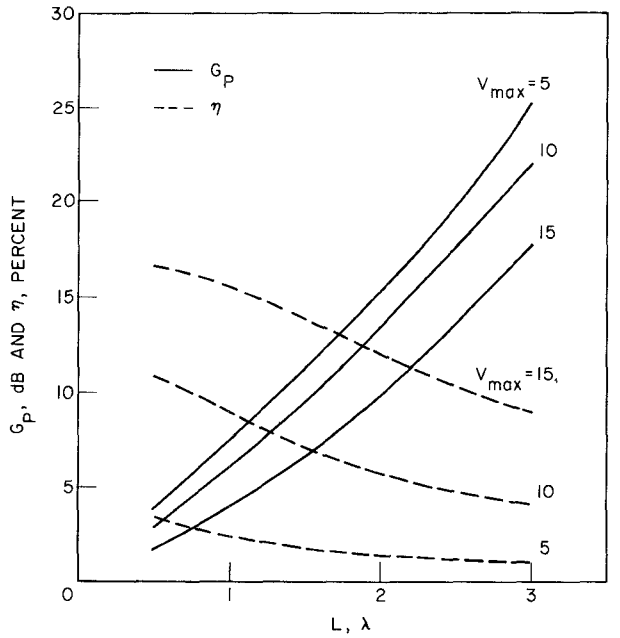

Fig. 8. Gain and efficiency for the amplifier case versus overall length for three different values of $(V_{RF})_{max}$ at the load. ($\rho_s = 5\times10^{-4}$ Ω − m, $d = 10$ μm).

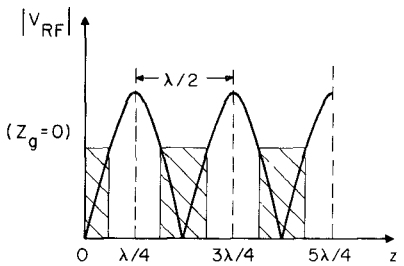

Fig. 9. Ideal RF voltage magnitude waveform for the shorted oscillator case with location of inactive regions indicated.

at the load. For each case, the output power is constant according to (11); for $(V_{RF})_{max} = 5$ V, it is $P_{RF} = 2.61$ W; for $(V_{RF})_{max} = 10$ V, $P_{RF} = 10.77$ W; and for $(V_{RF})_{max} = 15$ V, $P_{RF} = 24.72$ W. It is seen that the power gain increases with decreasing $(V_{RF})_{max}$; this is because $|G_D|$ is larger for smaller $(V_{RF})_{max}$. However, more power is generated in the line as $(V_{RF})_{max}$ increases so that maximum efficiency occurs for the $(V_{RF})_{max} = 15$ V case. If L is increased beyond 3λ, G_P continues to increase and η to decrease for each case; however, it becomes increasingly difficult to minimize reflections at the load so that the reflected power is small relative to the input power.

It is possible to increase the efficiency of the traveling-wave oscillator above the 11.2-percent value shown in Fig. 5. When referring to Fig. 6(a) for the shorted oscillator, it is seen that near integral multiples of λ/2, $|V_{RF}|$ is small and therefore little RF power is generated. However, dc power is still dissipated near $n\lambda/2$ points since the entire structure is biased into reverse breakdown. By making the semiconductor inactive in the vicinity of $n\lambda/2$ points ($n\lambda/2 + \lambda/4$ for the open oscillator), the device will not break down in these regions so that P_{dc} will be reduced.

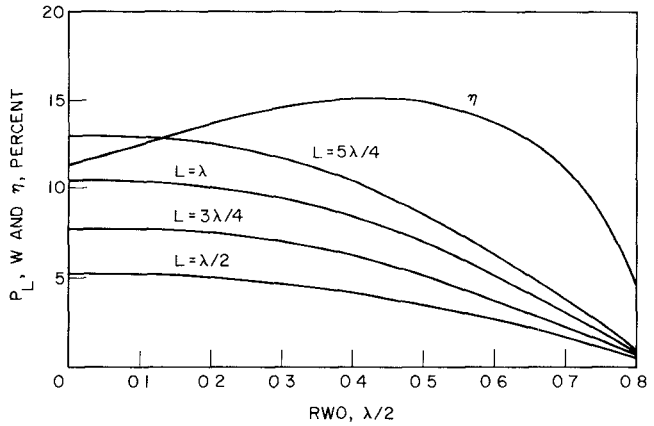

Fig. 10. Power output and efficiency versus inactive region width RWO for the oscillator case with $\rho_s = 5\times10^{-4}$ Ω − m, $d = 10$ μm for different oscillator lengths L.

P_{RF} at the load will also be reduced, but not by much since little RF power is generated near RF voltage nulls. Fig. 9 indicates how this may be done for the shorted oscillator, where the cross-hatched areas are inactive. If the shunt device capacitance is maintained about the same as before in these regions, additional reflection of traveling waves is minimized.

Fig. 10 shows the RF power and efficiency versus inactive region length (RWO in units of λ/2) for both shorted and open oscillators of different lengths. It is seen that the optimum inactive region length is 0.45λ/2, which increases the overall efficiency from 11.2 to 15 percent. It would not make sense to apply this technique to oscillators much longer than 5λ/4, since, according to Fig. 7, the RF voltage minima are far from zero as L increases.

It might be expected that, for large RWO values, the efficiency should approach that of the discrete device, in this case 25.46 percent. However, the value for the discrete device is obtained by assuming zero series parasitic resistance between the device and load. For the traveling-wave structure, the transmission-line sections connecting the active regions exhibit a nonzero series resistance which reduces the power delivered to the external load. Even for the case where the n^+ layer thickness d is reduced to zero, the metal exhibits a series resistance due to its finite conductivity and skin depth. In fact, the case for $d = 0$ was tried and it was found that the traveling-wave structure was not capable of delivering any power to the load due to the transmission-line series resistance and reduced series inductance. This result could be predicted from the lower limit on the substrate thickness d_L given in Table II.

Another method of increasing the efficiency of the oscillator was pointed out in [2]. Near voltage minima, the dc power may also be reduced by decreasing the width of the structure, w of Fig. 1.

IV. Conclusions

It has been shown that traveling-wave or distributed IMPATT devices are capable of generating significant amounts of RF power at reasonable terminating impedances and with reasonable efficiencies. Significantly higher

powers can be obtained from such structures as compared to discrete devices. There is a tradeoff, however, between power output and efficiency. The highest power outputs are obtained at lower efficiencies and, therefore, thermal limitations must be considered for these devices. Various techniques may be used to increase the overall efficiency, however, at the expense of power output.

Proper design of substrate width and resistivity is essential for traveling-wave devices. Formulas have been developed to determine the d_{opt} and ρ_s combination to yield the best efficiency for each IMPATT doping profile and desired operating frequency.

According to the transmission-line model adopted here, output power scales linearly with the device width (w in Fig. 1). However, as w is increased, transverse modes will become important and the equations used will no longer be applicable. Determining the effects of finite w requires an electromagnetic field analysis of the traveling-wave structure.

References

[1] T. A. Midford and H. C. Bowers, "A two-port IMPATT diode traveling wave amplifier," *Proc. IEEE*, vol. 56, pp. 1724–1725, Oct. 1968.

[2] K. G. Hambleton and P. N. Robson, "Design considerations for resonant traveling wave IMPATT oscillators," *Int. J. Elec.*, vol. 35, pp. 225–244, 1973.

[3] M. Franz and J. B. Beyer, "The traveling-wave IMPATT mode," *IEEE Trans. Microwave Theory Tech.*, vol. MTT-26, pp. 861–865, Nov. 1978.

[4] M. Franz and J. B. Beyer, "The traveling wave IMPATT mode: Part II—The effective wave impedance and equivalent transmission line," *IEEE Trans. Microwave Theory Tech.*, vol. MTT-28, pp. 215–218, Mar. 1980.

[5] B. Bayraktaroglu and H. D. Shih, "Millimeter-wave GaAs distributed IMPATT diodes," *IEEE Electron Device Lett.*, vol. EDL-4, pp. 393–395, Nov. 1983.

[6] Y. Fukuoka and T. Itoh, "Field analysis of a millimeter-wave GaAs double-drift IMPATT diode in the traveling-wave mode," *IEEE Trans. Microwave Theory Tech.*, vol. MTT-33, pp. 216–222, March 1985.

[7] R. K. Mains, G. I. Haddad, and P. A. Blakey, "Simulation of GaAs IMPATT diodes including energy and velocity transport equations," *IEEE Trans. Electron Devices*, vol. ED-30, pp. 1327–1338, Oct. 1983.

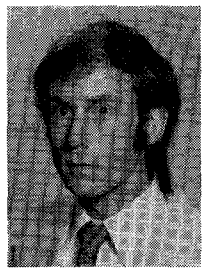

Richard K. Mains (S'79–M'79) was born in Chicago, IL, on March 28, 1950. He received the M.Sc. degree in electrical engineering in 1974 from the Ohio State University, Columbus, OH, and the Ph.D. degree in electrical engineering in 1979 from the University of Michigan, Ann Arbor.

He is presently working on microwave semiconductor device simulation at the Solid-State Electronics Laboratory, the University of Michigan.

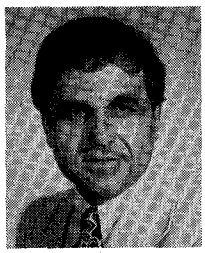

George I. Haddad (S'57–M'61–SM'66–F'72) was born in Aindara, Lebanon, on April 7, 1935. He received the B.S.E., M.S.E., and Ph.D. degrees in electrical engineering in 1956, 1958, and 1963, respectively, from the University of Michigan, Ann Arbor.

From 1957 to 1958, he was associated with the Engineering Research Institute of the University of Michigan, where he was engaged in research on electromagnetic accelerators. In 1958, he joined the Electron Physics Laboratory, where he has been engaged in research on masers, parametric amplifiers, detectors, electron-beam devices, and presently on microwave solid-state devices. He served as Director of the Laboratory from 1968 to 1975. From 1960 to 1969, he served successively as Instructor, Assistant Professor, and Associate Professor in the Electrical Engineering Department. He is currently a Professor and Chairman of the Department of Electrical and Computer Engineering.

Dr. Haddad received the 1970 Curtis W. McGraw Research Award of the American Society for Engineering Education for outstanding achievements by an engineering teacher. He is a member of Eta Kappa Nu, Sigma Xi, Phi Kappa Phi, Tau Beta Pi, the American Physical Society, and the American Society for Engineering Education.